

Implementation and testing of Lanczos-based algorithms for Random-Phase Approximation eigenproblems.

Myrta Grüning,^{1,2} Andrea Marini,^{3,4,5} and Xavier Gonze²

¹Centre for Computational Physics and Physics Department,
University of Coimbra, Rua Larga 3004-516 Coimbra, Portugal

²European Theoretical Spectroscopy Facility, NAPS/IMCN,
Université Catholique de Louvain, B-1348 Louvain-la-Neuve, Belgium

³European Theoretical Spectroscopy Facility, Physics Department, University ‘Tor Vergata’, I-00133 Rome, Italy

⁴Nano-Bio Spectroscopy Group, Universidad del País Vasco, E-20018 San Sebastián, Spain

⁵IKERBASQUE, Basque Foundation for Science, E-48011 Bilbao, Spain

The treatment of the Random-Phase Approximation Hamiltonians, encountered in different frameworks, like Time-Dependent Density Functional Theory or Bethe-Salpeter equation, is complicated by their non-Hermiticity. Compared to their Hermitian Hamiltonian counterparts, computational methods for the treatment of non-Hermitian Hamiltonians are often less efficient and less stable, sometimes leading to the breakdown of the method. Recently [Grüning et al. *Nano Lett.* **8**, 2820 (2009)], we have identified that such Hamiltonians are usually pseudo-Hermitian. Exploiting this property, we have implemented an algorithm of the Lanczos type for random-Phase Approximation Hamiltonians that benefits from the same stability and computational load as its Hermitian counterpart, and applied it to the study of the optical response of carbon nanotubes. We present here the related theoretical grounds and technical details, and study the performance of the algorithm for the calculation of the optical absorption of a molecule within the Bethe-Salpeter equation framework.

I. INTRODUCTION

The Random-Phase Approximation (RPA) Hamiltonian H^{RPA} appears in several areas of physics and theoretical chemistry, and describes strong collective excitations of a many-body system as the linear combination of particle-hole pairs $|\lambda\mu\rangle$ ^{1,2}. It has the form

$$H^{\text{RPA}} = \begin{pmatrix} R & C \\ -C^* & -R^* \end{pmatrix}, \quad (1)$$

where the resonant R and anti-resonant $-R^*$ blocks are Hermitian matrices in the subspace generated by particle-hole pairs propagating respectively forward ($|\lambda\mu\rangle$) and backward ($|\mu\tilde{\lambda}\rangle$) in time (in what follows α, λ indicate particles and β, μ holes), and the C and $-C^*$ blocks are symmetric matrices coupling the particle-hole pairs propagating forward and backward in time. The excitation energies and strengths of the many-body system are the eigensolutions of Eq. (1). Note that the RPA Hamiltonian is not Hermitian, thus its eigenvalues are not necessarily real.

In quantum chemistry, condensed matter physics, nanoscience, or nuclear physics, the RPA Hamiltonian appears within the state-of-the-art approaches for calculating the excitations in an electronic system: the time-dependent density functional theory³ (TD-DFT) and the Bethe-Salpeter⁴ (BS) equation.⁵ In the commonly used approximations to TD-DFT (e.g. real exchange-correlation kernel) and BS equation (static screening of the interaction), *all the eigenvalues are real*. TD-DFT is particularly successful for finite systems, namely molecules and molecular clusters, while the BS approach is mostly used for extended systems, like periodic bulk solids and, in general, for systems where excitonic ef-

fects play an important role⁶. Nowadays, the application of these approaches to the computation of the time-dependent responses of more and more complex systems, such as large bio-molecules or nanostructures, poses the problem of efficient solution of the eigenproblem for H^{RPA} . For large matrices, the direct diagonalization is usually not possible, and one has to resort to iterative algorithms, such as the Lanczos method. Such algorithms exist for both Hermitian and non-Hermitian Hamiltonian. However, compared to their Hermitian Hamiltonian counterparts, algorithms for the treatment of non-Hermitian Hamiltonians are often less efficient and less stable, sometimes leading to the breakdown of the method^{7,8}.

Within TDDFT, the very convenient Hermitian formulation of the eigenvalue problem proposed by Casida⁹ exists. However its application is limited to finite systems and purely local effective potentials for which the H^{RPA} is real. The presence of e.g. spin-orbit coupling prevents the application of Casida’s approach. In general a further approximation is introduced, the so-called Tamm-Dancoff approximation (TDA), that considers only particle-hole pairs propagating forward in time, so that the TDA Hamiltonian corresponds just to the resonant part, $H^{\text{TDA}} = R$. The TDA is often sufficiently accurate, as in the case of optical absorption spectra of periodic bulk systems. On the other hand, the TDA becomes inaccurate or even unphysical in the case of electron-energy-loss spectra¹⁰, reflectivity spectra¹¹, and also for the optical absorption of low-dimensional systems, e.g. nanosystems or π -conjugated molecules^{12,13}. In a previous work¹² we have implemented an approach for the solution of the RPA Hamiltonian, that avoids the TDA, and still benefits of the efficiency and robustness of the algorithms for the Hermitian case. This approach

has been already successfully applied to the calculation of the optical absorption and energy-loss spectra of a carbon nanotube. While our previous work focussed on the implications of the TDA for nanoscale systems, in this work the focus is on the theoretical grounds and some more technical aspects of that approach. We show here how the Lanczos algorithm for Hermitian eigenproblem (Sec. II A) can be used for the RPA Hamiltonian, that is pseudo-Hermitian with real eigenvalues (Sec. II C), by simply redefining the inner product (Sec. III A). We obtain (Sec. III B) the generalization to complex matrices of the scheme proposed by Van der Vorst in Ref. 14. The obtained algorithm is then further specialized (Sec. III C) to the calculation of the macroscopic dielectric function (from which the optical absorption and energy-loss spectra are derived) and finally applied to the calculation of the optical response of the trichloro-benzene isomers within the BS equation framework (Sec. IV), to show the algorithm accuracy (Sec. IV B) and efficiency (Sec. IV C).

II. MATHEMATICAL BACKGROUND

This section reviews briefly the two key “ingredients” of the presented approach: the Lanczos method for the solution of (non-)Hermitian eigenproblems, and the definition of pseudo-Hermitian matrix. The Lanczos method allows to calculate by recursion the eigenvalues, and eigenvectors, or directly the response spectrum, of large matrices. The pseudo-Hermiticity is related to the reality of the eigenvalues of a matrix and with the possibility of transforming the matrix into a Hermitian matrix.

A. Lanczos method for Hermitian eigenproblems

The Lanczos recursion method⁷ is a general algorithm for solving eigenproblems for a Hermitian operator H . This algorithm recursively builds an orthonormal basis $\{|q_i\rangle\}$ (Lanczos basis) in which H is represented as a real symmetric tridiagonal matrix,

$$T^k = \begin{pmatrix} a_1 & b_2 & 0 & \cdots & 0 \\ b_2 & a_2 & b_3 & & \vdots \\ 0 & \ddots & \ddots & \ddots & 0 \\ \vdots & & b_{k-1} & a_{k-1} & b_k \\ 0 & \cdots & 0 & b_k & a_k \end{pmatrix}. \quad (2)$$

The first vector $|q_1\rangle$ of the Lanczos basis is set equal to a (normalized) given vector $|u_0\rangle/\|u_0\|$. The next vectors are calculated from the three-term relation

$$|Q_{j+1}\rangle = H|q_j\rangle - a_j|q_j\rangle - b_j|q_{j-1}\rangle, \quad (3)$$

where

$$a_j = \langle q_j | H | q_j \rangle, \quad (4)$$

$$b_{j+1} = \|Q_{j+1}\|, \quad (5)$$

$$|q_{j+1}\rangle = |Q_{j+1}\rangle/b_{j+1}. \quad (6)$$

The algorithm is schematically described in Fig.(1). In

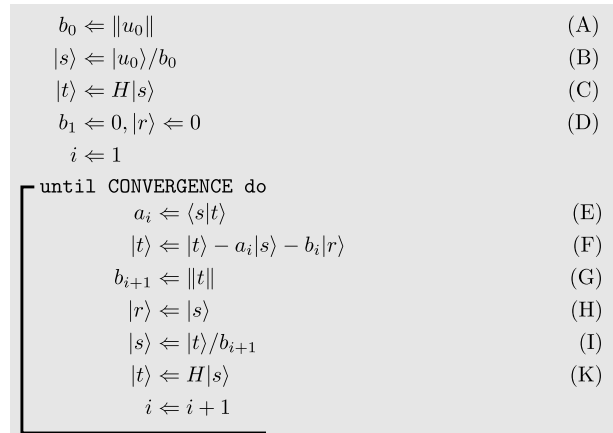


FIG. 1: Hermitian Lanczos algorithm

steps (A)-(D) the variables are initialized before entering the conditional loop [steps (E)-(K)]. Here, at each iteration a new vector of the Lanczos basis is computed till the convergence criteria is met. The cost per iteration is given mainly by the matrix-vector multiplication at step (K), that is of $O(N^2)$ for non-sparse matrices, with N the size of H . In terms of memory and storage, if one is just interested in the eigenvalues, at each iteration only three vectors ($|q_{n-1}\rangle, |q_n\rangle, |q_{n+1}\rangle$) are needed, and only two reals (a_i, b_i) need to be stored. At the end of the process one gets the tridiagonal matrix of Eq. (2) of dimension $k \times k$, that can be diagonalized with a cost $\propto k$. Compared with the standard diagonalization, the advantages are the memory usage, and the computational cost $\propto kN^2$ (for diagonalization is $O(N^3)$) as soon as the number of iterations $k \ll N$. This is in practice always the case when we are interested only in a portion of the spectrum of H .¹⁵

As first highlighted by Haydock^{16,17}, an additional advantage of Lanczos recursive approach is the possibility of calculating the resolvent $(\omega - H)^{-1}$ matrix elements, bypassing completely the diagonalization. In fact the resolvent for the state $|u_0\rangle$ takes the form of a continued fraction

$$\langle u_0 | (\omega - H)^{-1} | u_0 \rangle = \|u_0\|^2 \frac{1}{(\omega - a_1) - \frac{b_2^2}{(\omega - a_2) - \frac{b_3^2}{\ddots}}} \quad (7)$$

Other matrix elements can be then calculated by recursion (see A).

B. Lanczos method for non-Hermitian eigenproblems

The Lanczos recursive approach can be extended to the non-Hermitian case⁷. For a non-Hermitian matrix H , that we suppose diagonalizable, the action on a ket $|v\rangle$ differs from the action on a bra $\langle v|$: no orthogonal basis set exists, that could transform it into a diagonal form. The most straightforward extension of the Lanczos procedure illustrated in the previous subsection is the Arnoldi recursive approach that transforms H into an upper-Hessenberg matrix, instead of a tridiagonal one, and thus presents clear computational disadvantages with respect to the Hermitian case.¹⁸

It is still possible to tridiagonalize H , by defining a bi-orthonormal Lanczos basis $\{|p_i\rangle, |q_i\rangle\}$, that is $\langle p_i|q_j\rangle = \delta_{ij}$ while in general, $\{|p_i\rangle\}$, $\{|q_i\rangle\}$ are not orthogonal. In this basis, H is represented as a non-Hermitian tridiagonal matrix

$$T'^j = \begin{pmatrix} a_1 & b_2 & 0 & \cdots & 0 \\ c_2 & a_2 & b_3 & & \vdots \\ 0 & \ddots & \ddots & \ddots & 0 \\ \vdots & & c_{j-1} & a_{j-1} & b_j \\ 0 & \cdots & 0 & c_j & a_j \end{pmatrix}. \quad (8)$$

The first vectors, $\langle p_1|$, $|q_1\rangle$ of the Lanczos basis are set equal to given bi-orthonormal vectors $\langle w_0|$, $|u_0\rangle$. The next vectors are calculated from the three-term relations

$$|Q_{j+1}\rangle = (H - a_j)|q_j\rangle - c_j|q_{j-1}\rangle. \quad (9)$$

$$\langle P_{j+1}| = \langle p_j|(H - a_j^*) - \langle p_{j-1}|b_j. \quad (10)$$

where

$$a_j = \langle p_j|H|q_j\rangle, \quad (11)$$

$$b_{j+1} = \|Q_{j+1}\|, \quad (12)$$

$$c_{j+1} = \langle P_{j+1}|Q_{j+1}\rangle/b_{j+1}, \quad (13)$$

$$\langle p_{j+1}| = \langle P_{j+1}|/c_{j+1}, \quad (14)$$

$$|q_{j+1}\rangle = |Q_{j+1}\rangle/b_{j+1}. \quad (15)$$

Figure 2 schematically describes the algorithm corresponding to Eqs. (9,11). The number of steps is doubled with respect to the Hermitian case, since we build two sets of basis vectors, so that each operation performed for $|q_i\rangle$, has to be repeated for the $\langle p_i|$. Another important difference with respect to the Hermitian case is that, since $\{|p_i\rangle\}$, $\{|q_i\rangle\}$ are not orthogonal, it can happen that one of the new vectors that are built in Eqs. (9) are zero or their vector product is zero. Then at each iteration, one has to check, together with the convergence conditions, that the algorithm does not break down.¹⁹

Also the Lanczos-Haydock (LH) procedures, Eq. (7), can be generalized (b_i^2 are replaced by $c_i b_i$). Indeed, the non-Hermitian LH has been applied to the calculation of the dynamical polarizabilities of molecules within the time-dependent density functional and Bethe-Salpeter perturbation theory schemes introduced in Refs. 20–22.

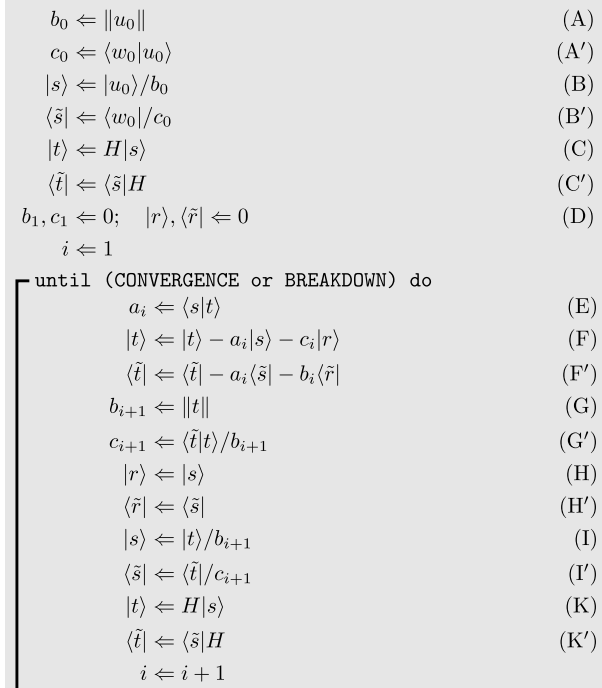


FIG. 2: Non-Hermitian Lanczos algorithm [Eqs. (9-15)]. The steps that are added with respect to the Hermitian case in Fig. (2), are tagged with a primed letter. See text for further explanations.

C. Pseudo-Hermiticity

The Hermiticity of an operator H , that is $H = H^\dagger$, insures the reality of the spectrum of H . However, Hermiticity is a sufficient, but not necessary condition for the reality of the spectrum of an operator. To study systematically non-Hermitian Hamiltonian with real spectrum, quite recently, Mostafazadeh²³ introduced the concept of pseudo-Hermiticity. The η -pseudo-Hermitian adjoint of H is defined as

$$H^\sharp := \eta^{-1}H^\dagger\eta \quad (16)$$

where η is an invertible transformation in Hilbert space. Then, a Hamiltonian is η -pseudo-Hermitian if $H^\sharp = H$. It is easy to recognize that this definition includes Hermiticity ($\eta = I$).

Using this concept, it is possible to define a sufficient as well as necessary condition for the reality of the spectrum of a matrix. It can be proved²⁴ that H diagonalizable has a real spectrum if and only if H is η -pseudo-Hermitian and there exists an operator O with $\eta = OO^\dagger$. Since η is positive-definite one can define an inner product,

$$\langle \cdot | \cdot \rangle_\eta := \langle \cdot | \eta \cdot \rangle, \quad (17)$$

and the corresponding norm $\|\cdot\|_\eta$. Then, with respect to this inner product, H is Hermitian (alternatively O transforms H into an Hermitian Hamiltonian).

III. PSEUDO-HERMICITY OF THE RPA HAMILTONIAN

In this section we first show that the RPA Hamiltonian is pseudo-Hermitian, and introduce an operative way to define the inner product with respect to which H^{RPA} is Hermitian. As a consequence, the Lanczos algorithm for Hermitian operators presented in the previous section is simply reformulated using this inner product. Finally the algorithm is specialized for TD-DFT and BS calculations of excited state properties of electronic systems.

A. Redefinition of the inner product for RPA Hamiltonian

The RPA Hamiltonian H can be written as^{2,25}

$$H = F\bar{H} = \begin{pmatrix} 1 & 0 \\ 0 & -1 \end{pmatrix} \begin{pmatrix} R & C \\ C^* & R^* \end{pmatrix}. \quad (18)$$

In Eq. (18), F is a Hermitian involution, and \bar{H} a Hermitian matrix (indeed R is Hermitian, and C is symmetric). H is pseudo-Hermitian with respect to both F and \bar{H} . In fact, since F is an involution, $\bar{H} = FH$, and the F -pseudo-Hermicity, $FH = H^\dagger F$ follows directly from the Hermicity of \bar{H} . Note that the F -pseudo-Hermicity corresponds to the invariance of the Hamiltonian with respect to FK , with K is the complex conjugation matrix, or more physically to the invariance of the Hamiltonian under the combined action of parity (F) and time-reversal (K) operator. However, since F is clearly non positive definite, it cannot be used for defining a norm.

More interestingly, the \bar{H} -pseudo-Hermicity is also easily proved

$$\begin{aligned} \bar{H}H &= FHH && (\bar{H} \text{ definition}) \\ &= H^\dagger FH && (\bar{H} \text{ } F\text{-pseudo-Hermicity}) \\ &= H^\dagger \bar{H} && (\bar{H} \text{ definition}) \quad \square. \end{aligned}$$

The positive definitiveness of \bar{H} is intimately related to the nature of the independent particle solution $|\Phi\rangle$ from which the particle-hole pairs are built. In fact \bar{H} is the curvature tensor, or stability matrix, that one obtains when expanding the energy surface around the stationary point $|\Phi\rangle$ for small variations $|\delta\Phi\rangle$. If $|\Phi\rangle$ corresponds to a minimum in the energy surface, then \bar{H} is positive definite.² For excitations of an electronic system, in connection with the singlet-triplet instability, Zimmermann²⁵ found that a sufficient condition for \bar{H} to be positive definite is the smallest particle-hole pair energy being larger than the modulus of the largest matrix element of the coupling matrix C .

Except in very rare cases, in practical applications the $|\Phi\rangle$ corresponds to a minimum in the energy surface, hence we can use \bar{H} to define a modified inner product, with respect to which H is Hermitian

$$\langle \cdot | \cdot \rangle_{\bar{H}} := \langle \cdot | \bar{H} \cdot \rangle, \quad (19)$$

and the associate norm. With this inner product, the closure relation for a complete set of functions $\{\Psi_n\}$, orthonormal with respect to the modified inner product, has to be defined accordingly as

$$\sum_n \bar{H} |\Psi_n\rangle \langle \Psi_n| = I. \quad (20)$$

B. Lanczos recursive method for RPA Hamiltonians

Using the properties in previous section, we can redesign the Lanczos recursive procedure (Sec. II A) simply by replacing the standard inner product with the one defined in Eq. (19). The result is the algorithm proposed in Ref.14 generalized to complex matrices. The main question is whether the replacement of the inner product is convenient numerically, with respect to the standard non-Hermitian Lanczos method. Indeed the new inner product implies a matrix-vector multiplication by \bar{H} , and thus, as in the non-Hermitian Lanczos, the computational cost is doubled. However, taking into account that \bar{H} and H are related by F , effectively only one matrix-vector multiplication is needed as in the Lanczos method for Hermitian matrices. In fact,

$$a_j = \langle q_j | H q_j \rangle_{\bar{H}} = \langle q_j | H^\dagger F H | q_j \rangle = \langle (H q_j) | F | (H q_j) \rangle, \quad (21)$$

$$b_{j+1} = \|Q_{j+1}\|_{\bar{H}} = \sqrt{\langle Q_{j+1} | F | (H Q_{j+1}) \rangle}, \quad (22)$$

so that only one matrix-vector multiplication by H appears, while computing the matrix elements of F will be unexpensive, because F corresponds to the identity in the subspace of particle-hole propagating forward in time and to minus the identity in the subspace of particle-hole propagating backward in time. The Lanczos algorithm so modified is shown in Fig. 3. With respect to the Hermitian case both in the variable initialization [steps (A) to (F)], and in the conditional loop [steps (G) to (O)] the algorithm is rearranged: the b_i factors [steps (C) and (M)] are calculated after the matrix-vector multiplication [steps (B) and (L)]; as a consequence two additional steps are added to normalize the Lanczos basis vectors [steps (D)-(E), (N)-(O)]. The reordering, and addition of the extra (computationally inexpensive) steps avoids the additional matrix-vector multiplication due to the modified inner product. The cost is then, as in the Hermitian case, of one vector-matrix multiplication. Coming to the diagonal matrix elements of the resolvent for the state $|u_0\rangle$ [Eq. (7) in the Hermitian case], the straightforward generalization (that is substituting the standard with the \bar{H} -inner product) gives

$$\langle u_0 | (\omega - H)^{-1} u_0 \rangle_{\bar{H}} = \|u_0\|_{\bar{H}}^2 \frac{1}{(\omega - a_1) - \frac{b_2^2}{(\omega - a_2) - \frac{b_3^2}{\dots}}}. \quad (23)$$

```

|s⟩ ← |u₀⟩ (A)
|t⟩ ← H|s⟩ (B)
b₀ ← √⟨s|F|t⟩ (C)
|s⟩ ← |s⟩/b₀ (D)
|t⟩ ← |t⟩/b₀ (E)
b₁ ← 0, |r⟩ ← 0 (F)
i ← 1

until CONVERGENCE do
  aᵢ ← ⟨t|F|t⟩ (G)
  |t⟩ ← |t⟩ - aᵢ|s⟩ - bᵢ|r⟩ (H)
  |r⟩ ← |s⟩ (I)
  |s⟩ ← |t⟩ (K)
  |t⟩ ← H|s⟩ (L)
  bᵢ₊₁ ← √⟨s|F|t⟩ (M)
  |s⟩ ← |s⟩/bᵢ₊₁ (N)
  |t⟩ ← |t⟩/bᵢ₊₁ (O)
  i ← i + 1

```

FIG. 3: Pseudo-Hermitian Lanczos algorithm

However, we are still interested in the matrix element calculated with the standard inner product. Using the closure relation [Eq. (20)], we expand $\langle w_0 | (\omega - H)^{-1} | u_0 \rangle$ in terms of $\langle q_i | (\omega - H)^{-1} | u_0 \rangle_{\bar{H}}$,

$$\langle w_0 | (\omega - H)^{-1} | u_0 \rangle = \sum_i \langle w_0 | q_i \rangle \langle q_i | (\omega - H)^{-1} | u_0 \rangle_{\bar{H}}. \quad (24)$$

The first element of the sum $\propto \langle u_0 | (\omega - H)^{-1} | u_0 \rangle_{\bar{H}}$ is given by Eq. (23), while the other elements are found by recursion (see A). The standard product $\langle w_0 | q_i \rangle$, can be computed at each iteration of the Lanczos process and stored. The elements with $i \neq 1$ are different from zero, since the Lanczos basis vectors are orthonormal with respect to the \bar{H} -inner product, not with respect the standard one. On the other hand for the cases we studied we found that in fact the summation in Eq. (24) converges rapidly.

C. Special case of calculation of the macroscopic dielectric function

The Lanczos approach introduced in the previous subsection can be applied to calculate the macroscopic dielectric function $\epsilon_M(\omega)$ within either the BS or TD-DFT framework. As shown in Ref. 26 the $\epsilon_M(\omega)$ can be rewritten as

$$\epsilon_M(\omega) = 1 - \langle P | (\omega - H)^{-1} F | P \rangle, \quad (25)$$

where $|P\rangle$ is a ket whose components in the $|\lambda\mu\rangle$ and $|\mu\lambda\rangle$ space are the optical oscillators: $\langle P | \lambda\mu \rangle \propto \langle \lambda | \vec{d} \cdot \vec{\xi} | \mu \rangle$, with \vec{d} the electronic dipole, and $\vec{\xi}$ the light polarization factor. The components of the $|P\rangle$ vector in a particle-hole pair basis have the following symmetry

$$\langle \mu\lambda | P \rangle = (\langle \lambda\mu | P \rangle)^*. \quad (26)$$

Eq. (25) is straightforwardly calculated from Eq. (24) choosing $|u_0\rangle = F|P\rangle$. The components of $|u_0\rangle$ vector in a particle-hole pair basis have the following symmetry

$$\langle \mu\lambda | u_0 \rangle = -(\langle \lambda\mu | u_0 \rangle)^*. \quad (27)$$

The symmetry property of $|u_0\rangle$ [Eq. (27)] can be used to further reduce the computational load of the pseudo-Hermitian Lanczos algorithm. Within the vector space spanned by the particle-hole pairs let's consider the subspace \mathcal{V}_- of vectors with the property Eq. (27), and the subspace of vectors \mathcal{V}_+ with the property Eq. (26). The two subspace are clearly non-overlapping. It can be verified that \bar{H} transforms a vector $v \in V_{+(-)}$ in a vector w belonging to the same subspace, while F transforms a vector $v \in V_{+(-)}$ in a vector w' belonging to the other subspace. As a consequence H transforms a vector $v \in V_{+(-)}$ in a vector w' belonging to the other subspace. Also, we note that when q_j belongs to either one of the subspace, the product in Eq. (21) is zero.

Next, using Eq. (3) it can be demonstrated by induction that if the first Lanczos basis vector $|q_1\rangle$ belongs to one of the subspaces, the vectors of the Lanczos basis set belongs to either one of the subspaces depending on the parity of the iteration j . More specifically if—as it is our case— $|q_1\rangle \in \mathcal{V}_-$, then all $|q_j\rangle$ with j odd belong to \mathcal{V}_- , and all q_j with j even belong to \mathcal{V}_+ . In fact, if $q_1 \in \mathcal{V}_-$ then $q_2 \in \mathcal{V}_+$ (base case). Furthermore, suppose that in Eq. (3), $|q_j\rangle \in \mathcal{V}_-$, and $|q_{j-1}\rangle \in \mathcal{V}_+$, then Q_{j+1} (thus the normalized q_{j+1}) belong to \mathcal{V}_+ and Q_{j+2} [obtained by applying again Eq. (3) after updating $|q_{n-1}\rangle, |q_n\rangle, |q_{n+1}\rangle$] to \mathcal{V}_- (inductive step).

```

|s⟩ ← |λμ⟩⟨λμ|u₀⟩ (A)
|t⟩ ← R|s⟩ - C|s⟩* (B)
b₀ ← √2Re⟨s|t⟩ (C)
|s⟩ ← |s⟩/b₀ (D)
|t⟩ ← |t⟩/b₀ (E)
b₁ ← 0, |r⟩ ← 0 (F)
i ← 1

until CONVERGENCE do
  |t⟩ ← |t⟩ - bᵢ|r⟩ (G)
  |r⟩ ← |s⟩ (H)
  |s⟩ ← |t⟩ (I)
  |t⟩ ← R|s⟩ + (-1)ᵢ⁺¹C|s⟩* (K)
  bᵢ₊₁ ← √2Re⟨s|t⟩ (L)
  |s⟩ ← |s⟩/bᵢ₊₁ (M)
  |t⟩ ← |t⟩/bᵢ₊₁ (N)
  i ← i + 1

```

FIG. 4: Pseudo-Hermitian Lanczos algorithm modified to account for a starting vector $|P\rangle$ with the anti-Hermitian property given by Eq. (27)

Figure 4 shows the modified Lanczos algorithm for the case in which the starting vector has the symmetry property given by Eq. (27). Since half of the components of

$|u_0\rangle$ contains all the information, the first Lanczos vector [step (A)] is just the projection $|u_0\rangle$ on the $|\lambda\mu\rangle$ subspace (that is only particle-hole pairs propagating forward in time). Then, if H^{RPA} is a $N \times N$ matrix, the algorithm works with vectors and matrices of dimension $N/2$ and $N/2 \times N/2$ respectively, like in the case of the TDA approximation. The multiplication by H^{RPA} , that is the operation determining the cost of the algorithm, is replaced by two matrix-vector multiplications for matrices of half the size [steps (B) and (K)], so that the cost is reduced by a factor two compared to the full matrix case.²⁷

Similarly, the \bar{H} -norm of a vector defined in Eq. (22) is rewritten as in steps (C) and (L) of Fig. 4. Furthermore, since all a_i are zero by symmetry they do not need to be calculated and can be omitted [step (G)] in the three-terms relation [Eq. (3)].

IV. RESULTS

We applied the algorithms described in Figs. (1) and (4) to the calculation of the optical absorption of the isomers of the trichlorobenzene (TCB) molecule within the BSE framework. First, we analyze the effect of the TDA on the spectra of the isomers, then we assess the accuracy and efficiency of the algorithms.

A. Effect of the particle-hole hole-particle coupling

Within the BSE framework the R and C matrix elements are defined as

$$R_{\alpha\beta,\lambda\mu} = (E_\beta - E_\alpha)\delta_{\alpha\lambda}\delta_{\beta\mu} + K_{\alpha\beta,\lambda\mu}, \quad (28)$$

$$C_{\alpha\beta,\mu\lambda} = K_{\alpha\beta,\mu\lambda}, \quad (29)$$

where E_α, E_β are the (quasi)particle/hole energies. The BS kernel (see e.g. Ref. 6)

$$K_{\alpha\beta,\lambda\mu} = \bar{v}_{\alpha\beta,\lambda\mu} - W_{\alpha\beta,\lambda\mu}, \quad (30)$$

describes the interaction between the particle-hole pairs in terms of particle-hole exchange $\bar{v}_{\alpha\beta,\lambda\mu}$ (\bar{v} is the Hartree potential without the long-range component) and attraction $W_{\alpha\beta,\lambda\mu}$ (W is the screened interaction). The particle-hole exchange is responsible of the local-field effects, that is the effect of the induced microscopic electric fields. The particle-hole attraction introduces instead the so-called excitonic effects.

In our calculations the basis of particle-hole pairs $\{|\gamma\lambda\rangle\}$ has been obtained from the solution of the Kohn-Sham equation for the system. The Kohn-Sham orbital energies has been corrected to obtain the (quasi)particle/hole energies E_α, E_β by using the GW approximation. The Kohn-Sham calculations have been performed using the pseudo-potential plane-wave code ABINIT²⁸, while the GW and BSE calculations have been performed using the YAMBO code²⁹ where the algorithms described in this work have been implemented.

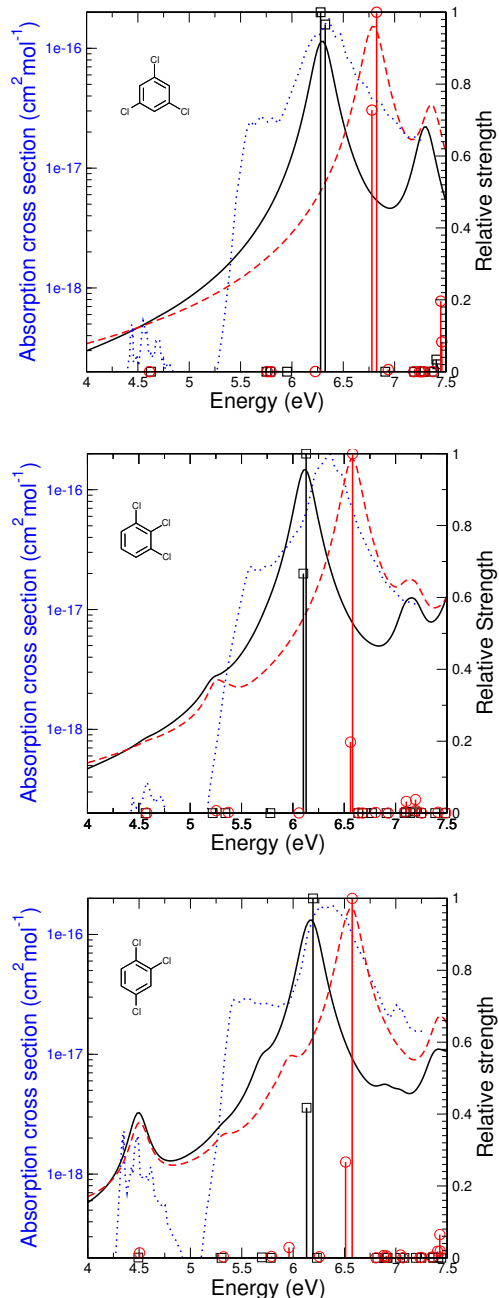


FIG. 5: [Color online] Optical spectra of TCB isomers: 1,3,5-TCB (top panel), 1,2,3-TCB (middle panel), 1,2,4-TCB (bottom panel). The imaginary part of the macroscopic dielectric function (in arbitrary unit) calculated within BSE using both full (black solid line) and TDA (red dashed line) are compared with the gas-phase experimental absorption cross section spectra (blue dotted line). The energy and relative strength of the excitations for full BSE (black squares) and TDA-BSE (red circles) obtained by exact diagonalization are reported in linear scale (the largest intensity is normalized to 1).

Figure 5 shows the optical absorption spectra of 1,3,5-TCB, 1,2,3-TCB and 1,2,4-TCB within the BSE obtained both by LH and exact diagonalization of either the TDA or the full Hamiltonian. Results are compared with the gas-phase experimental absorption cross section.³⁰ The experimental spectra for the three isomers are very similar to each other with the main peak centered at about 6.3 eV, a shoulder at about 5.5 eV and a very weak feature at 4.5 eV. For 1,2,4-TCB, the isomer with less symmetry, the peak at 4.5 eV is enhanced, the shoulder is broader and more pronounced and an extra peak is visible at 7 eV. The full BSE spectrum reproduces fairly well the position of the peaks in the three isomers. 1,3,5-TCB, 1,2,3-TCB show a dark transition at 4.5 eV, that acquires strength for the 1,2,4-TCB. In correspondence of the 5.5 eV shoulder in the experimental spectra, all the theoretical spectra present excitations. In the 1,3,5-TCB these are dark, while for 1,2,3-TCB and 1,2,4-TCB a shoulder appears in the spectra. The theoretical spectrum of 1,2,4-TC shows also the additional peak around 7 eV. The neglect of the coupling within the TDA blue-shifts by about 0.5 eV the main peak for all the isomers, with the effect of worsening the agreement with the experimental data, especially for what concern the relative position of the peaks. The main peak is due to two very close excitations due mostly to the $\pi \rightarrow \pi^*$ transitions between the doubly degenerate highest occupied (HOMO) and the doubly degenerate lowest unoccupied molecular orbital (LUMO) and is delocalized over the whole molecule. The analysis of the particle-hole pairs needed to describe these excitations show an important contribution coming from the particle-hole pair with negative energy at minus the HOMO-LUMO gap, that is neglected within the TDA. These results confirm the trend of blue-shifting and overestimating the intensity of excited state with a more delocalized character (such as $\pi \rightarrow \pi^*$ excitations in molecules) that has been already observed and discussed in the literature.^{12,13}

B. Accuracy of the pseudo-Hermitian Lanczos algorithm

At each iteration the LH algorithm provides an approximation for the eigenvalue spectrum of the RPA Hamiltonian and thus, through the macroscopic dielectric function, of the optical absorption spectrum. Figure 6 shows how by increasing the number of iterations, the spectrum obtained by the LH approach becomes more and more accurate, until the results are, for about 300 iterations, indistinguishable on the scale of the plot. Note that the spectrum does not converge uniformly for all energies, but it converges before in the low energy part, and then progressively for higher excitations. In fact if we restrict ourselves to the part of the spectrum examined in the experiment would need only about 75 iterations.

The accuracy can be improved by properly terminating the continued fraction in Eqs. (7, 24). For the spectra in

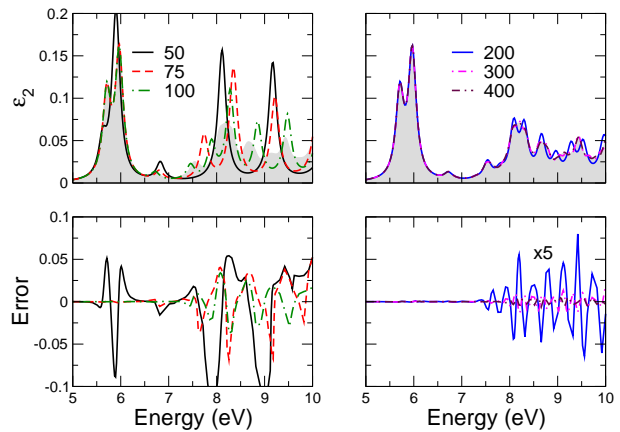


FIG. 6: [Color online] Top panels: Absorption spectrum of 1,3,5-TCB obtained by exact diagonalization (gray shadow) or by the LH iterative procedure for a different number of iterations. Bottom panels: error in spectrum obtained by the LH method with respect to exact diagonalization. Note that in the right bottom panel the curve have been magnified by a factor 5. The matrix elements in Eqs. (28) of the Hamiltonian have been calculated with $W_{\alpha\beta,\lambda\mu} = 0$ in Eq. (30) and without quasiparticle corrections.

Fig. 6 we just truncated the continued fraction. Instead, as suggested in Ref. 21, in Fig. 7 the asymptotic behavior of the continued fraction is described by the terminator

$$g(\omega) = \frac{\omega^2 + b_u^2 - b_g^2 + \sqrt{(\omega^2 + b_u^2 - b_g^2)^2 - 4\omega^2 b_u^2}}{2\omega b_u^2}, \quad (31)$$

that is obtained by resumming the continued fraction corresponding to a tight-binding Hamiltonian with the hopping parameters oscillating between two values, b_u and b_g .³² For b_u and b_g we use the averages of the odd and even b_i in Eq. (2) respectively. In fact we have verified that in Eq. (2) the odd (even) b_i oscillate around its asymptotic value b_u (b_g).³³

The terminator improves the quality of the spectrum obtained by iteration especially for higher energies (as it should be since we are correcting the asymptotic behavior) where it partially eliminates the spurious oscillations due to the truncation of the continued fraction. Using the terminator we then reduce to 200 the number of iterations needed for satisfactorily reproducing the exact diagonalization results in the whole energy range we considered.

C. Efficiency of the pseudo-Hermitian Lanczos algorithm

The computational time is determined by two factors: the dimension of the Hamiltonian and the number of iterations needed to reach a desired accuracy. First, we analyze the behavior of the algorithm with respect to the dimension of the Hamiltonian. Figure 8 compares

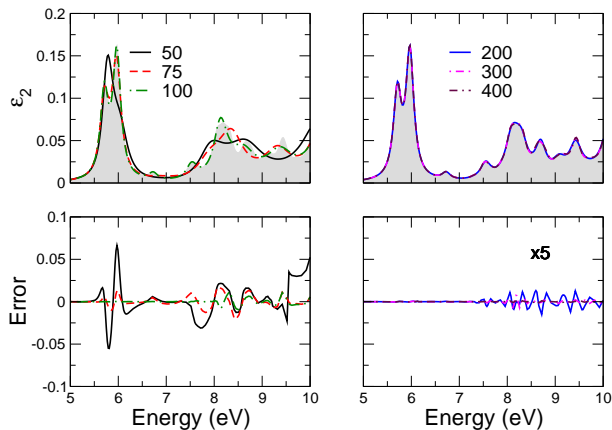


FIG. 7: As Fig. 6, but the terminator in Eq. (31) has been used for the continued fraction in Eqs. (7, 24).

the timing for exact and iterative diagonalization of the BSE using the LH approach, either including (pseudo-Hermitian H) or neglecting (Hermitian H) the coupling. The number of particle-hole pairs has been gradually increased so to enlarge the dimension of the Hamiltonian. Note that for the TDA Hamiltonian the dimension is equal to the particle-hole pairs, while for the full Hamiltonian the dimension is equal to twice the particle-hole pairs. For the LH approach the number of iteration is kept fixed.

When the number of particle-hole pairs exceeds 1000, the iterative methods become faster than exact diagonalization: for about 7000 particle-hole pairs the LH iterative procedure is about two order of magnitude faster for the Hermitian case, and three order of magnitude faster for the pseudo-Hermitian case. In fact, the computational time of diagonalization is increasing rapidly with the dimension of the matrix, it grows about two order of magnitude while the Hamiltonian grows by about one order of magnitude. On the other hand the computational time of the LH approach is increasing slowly with the dimension of the matrix, while the Hamiltonian dimension grows of one order of magnitude, the computation time remains of the same order of magnitude. Note that the non-Hermiticity has large impact on the timing of the diagonalization, while—thanks to the algorithm presented in Fig. 4—it does not influence the performance of the iterative method considering that the full Hamiltonian has twice the dimensions if the TDA one.

Second, we turn to the number of iterations needed to fulfill a given convergence criterium. Figure 9 compares, fixed the dimension of the Hamiltonian, the error on the spectrum with the number of iteration in the Hermitian and pseudo-Hermitian case. We measured the error at each iteration j as the frequency-weighted sum (on all the frequencies within the considered energy range) of the differences with respect to the previous iteration $\sum_i |S_i(j) - S_i(j-1)|/S_i(j)/\omega_i$, where S_i is the value of the spectrum at ω_i .³⁴ It appears that the LH approach applied to the Hermitian TDA Hamiltonian converges to

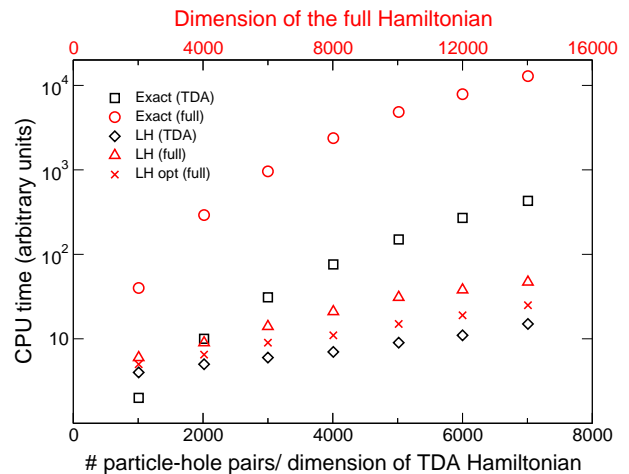


FIG. 8: Time needed to diagonalize the Hamiltonian against the number of particle-hole pairs, either by exact diagonalization (using the LAPACK from the Intel Mathematical Kernel Library) or by the LH method (200 iterations, 1500 frequencies in the range between 0-15 eV). For the TDA Hamiltonian, the LH in Fig. (1) has been used. For the full Hamiltonian both the pseudo-Hermitian LH in Fig. (3) and the optimized pseudo-Hermitian LH in Fig. (4) have been used. The CPU time (one core on an Intel/Xeon) has been measured using standard C timing routines.

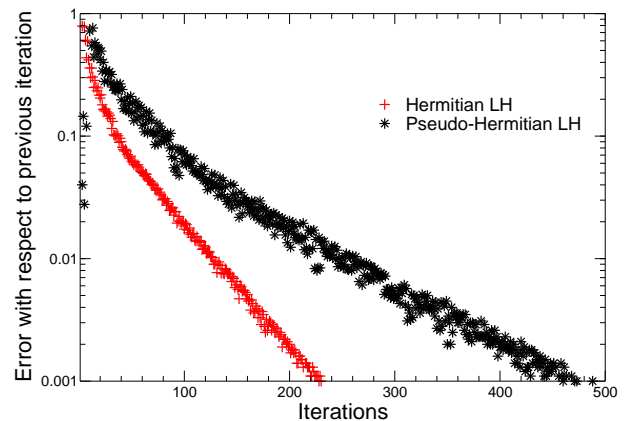


FIG. 9: Fixed the Hamiltonian dimension ($N=4824$), convergence behavior with the number of iterations of the Hermitian and pseudo-Hermitian LH.

a given threshold about twice as fast than the LH approach for the full Hamiltonian. In order to explore the causes of the slower convergence for the full Hamiltonian, we have considered the Hermitian Hamiltonian

$$H^{\text{no coupl}} = \begin{pmatrix} R & 0 \\ 0 & -R^* \end{pmatrix} \quad (32)$$

obtained by setting the coupling elements to zero in Eq. (1), and we have diagonalized it using both the Hermitian and the pseudo-Hermitian LH algorithms. In both cases we found the convergence rate is the same as for the full Hamiltonian with the coupling. This indicates that neither the coupling/non-Hermiticity, neither the pseudo-

Hermitian algorithm are responsible for the slower convergence rate. We conjecture that the difference is due to different spectrum of the TDA Hamiltonian and the $H^{\text{no coupl}}$. In Ref. 31, Chen and Guo have shown for the simple Lanczos that fixed the number of iterations k , the number of converged eigenvalues m in the Lanczos method was inversely proportional to the spectral range r of the Hamiltonian (defined as $r = E_{\text{max}} - E_{\text{min}}$, where $E_{\text{max/min}}$ is the largest/smallest eigenvalue of H). Considering our particular case, the energy spectrum of R in $H^{\text{no coupl}}$ goes from (approximative estimate from independent particle energies) 4.4 eV to 27 eV, instead the energy spectrum of R' (of the same dimension N as $H^{\text{no coupl}}$) goes from 4.4 eV to 28 eV³⁵ So practically the energy range of R and R' is very similar, and the energy range of $H^{\text{no coupl}}$ goes from -27 eV to 27 eV, that is about twice as large than that of R' . This may explain the slower convergence rate of the LH method for $H^{\text{no coupl}}$.

V. SUMMARY

In this work we have explained the theoretical ground and detailed the derivation of the pseudo-Hermitian Lanczos recursion method for RPA Hamiltonian introduced in Ref. 12. We also discussed, using numerical examples, the accuracy and the computational cost of the method when compared with conventional diagonalization techniques and the Hermitian Lanczos recursion method. As expected the cost per iteration of the Hermitian and pseudo-Hermitian (at parity of matrix dimension) is the same. On the other hand the number of iterations needed to reach a desired accuracy in the Lanczos eigenvalues spectrum is larger (about the double) of the Hermitian case. We have tested that this behavior does not depend on either the non-Hermiticity of the Hamiltonian or the pseudo-Hermitian algorithm: we argue that it is caused by the larger spectral range. In fact the RPA spectra includes both negative and positive particle-hole pairs, thus it is about the double of the TDA spectra. We expect the pseudo-Hermitian LH algorithm for the RPA to have particular relevance within computational condensed matter physics and theoretical chemistry, where the calculation of the optical response of materials require the solution of large eigenproblems for RPA Hamiltonian. In fact, as shown briefly in this work, and discussed in Ref. 10,12,13, the treatment of the full RPA Hamiltonian is important for accurately reproducing optical spectra of molecules, nanostructures and the energy loss function in solids. Moreover by using the pseudo-Hermiticity property it is possible in principle to conveniently reformulate any Hermitian algorithm for RPA eigenproblems.

Acknowledgments

M. G. acknowledges the usage of computer resources at the Laboratory for Advanced Computing of the University of Coimbra and is grateful to the Fundação para a Ciência e a Tecnologia (FCT) for its support through the Ciência 2008 programme. A. M. thanks the HPC-Europa2 Transnational mobility program (RII3-CT-2003-506079). X. G. acknowledges support from the Belgian State - Belgian Science Policy through the Interuniversity Attraction Poles Program (P6/42), the EU's 7th Framework Programme through the ETSF I3 e-Infrastructure project (Grant Agreement 211956), the Walloon region Belgium (RW project N° 816849, WALL-ETSF), FRS-FNRS Belgium (FRFC Grant N° 2.4.589.09.F), the Agentschap voor Innovatie door Wetenschap en Technologie (IWT project N° 080023, ISIMADE), and the Communauté française de Belgique through the NANHYMO project (ARC 07/12-003).

Appendix A: Off-diagonal resolvent matrix elements in the Lanczos basis

The off-diagonal resolvent matrix elements in the Lanczos basis at iteration j ,

$$G_{i,0}^j = \langle q_i | (\omega - H)^{-1} | u_0 \rangle, \quad (\text{A1})$$

can be obtained by recursion considering the system of linear equation

$$(\omega I - T^j) G_{i,0}^j = \delta_{i,0}, \quad (\text{A2})$$

with T^j defined in Eq. (2) from which it follows

$$G_{1,0}^j = (1 - (\omega - a_1)G_{0,0}^j)/b_2, \quad (\text{A3})$$

$$G_{n,0}^j = (-b_n G_{n-2,0}^j - (\omega - a_n)G_{n-1,0}^j)/b_{n+1}. \quad (\text{A4})$$

Alternatively, by direct solution of Eq. (A2) one obtains

$$G_{n,0}^j = (-1)^n \prod_{i=1}^n b_{i+1} \frac{|A_{n+1}^j|}{|A_0^j|}. \quad (\text{A5})$$

where $A^j = \omega I - T^j$, and A_i^j is the minor of A^j obtained by deleting the first i rows and columns. This expression can be rewritten to obtain a recursion formula as,

$$G_{n,0}^j = -b_{n+1} \frac{|A_{n+1}^j|}{|A_n^j|} G_{n-1,0}^j. \quad (\text{A6})$$

Equations (A6) and (A4) are equivalent [using $G_{00}^j = |A_1^j|/|A_0^j|$ and the relation $|A_i^j| = (\omega - a_{i+1})|A_{i+1}^j| - b_{i+2}^2|A_{i+2}^j|$ in Eq. (A4), one obtains Eq. (A6)], but they may give different results due to the propagation of numerical error. In fact, since Eq. (A4) depends on ω , the

error δ on $G_{0,0}^j$ propagates and affects $G_{n,0}^j$ by about $(\omega)^{n+1}\delta$. Eq. (A6) instead, the error on $G_{n,0}^j$ is proportional to $(|A_{n+1}|/|A_1|)\delta$. From numerical test we have seen that Eq. (A4) gives indeed numerical problems

for large n , thus Eq. (A6) has been used to calculate the off-diagonal resolvent matrix elements in Eq. (23). Since $|A_{n+1}^j|/|A_n^j|$ are computed already to obtain $G_{0,0}^j$, Eq. (A6) does not introduce extra computational cost.

-
- ¹ A. L. Fetter and J. D. Walecka, *Quantum Theory of many-particle systems* (Dover, 2003), chap. 15, p. 565.
- ² P. Ring and P. Schuck, *The Nuclear Many-Body Problem (Theoretical and Mathematical Physics)* (Springer, 1980), chap. 7,8, p. 244.
- ³ E. Runge and E. K. U. Gross, Phys. Rev. Lett. **52**, 997 (1984).
- ⁴ E. E. Salpeter and H. A. Bethe, Phys. Rev. **84**, 1232 (1951).
- ⁵ Because of the 4-point nature of the kernel, within BS the reformulation in terms of the eigenproblem for H^{RPA} is the only feasible alternative. To the contrary, within TD-DFT the direct solution of the Dyson-like equation is affordable and even the most convenient in the case of bulk periodic systems. On the other hand, for finite or sparse systems even within TDDFT the solution of the eigenproblem for \mathbf{H}^{RPA} can be more efficient than the direct solution especially when one is interested only to a frequency range where the excitations are well separated.
- ⁶ G. Onida, et al., Rev. Mod. Phys. **74**, 601 (2002).
- ⁷ *Templates for the solution of algebraic problems: a practical guide*, edited by Z. Bai, J. Demmel, J. Dongarra, A. Ruhe, H. van der Vorst, (SIAM, Philadelphia, 2000).
- ⁸ S. Tretiak, C. M. Isborn, A. M. N. Niklasson, and M. Chalacombe J. Chem. Phys. **130**, 054111 (2009)
- ⁹ M. Casida, in *Recent Advances in Density Functional Methods*, edited by D. P. Chong (World Scientific, Singapore, 1995), vol. 1.
- ¹⁰ V. Olevano and L. Reining, Phys. Rev. Lett. **86**, 5962 (2001).
- ¹¹ A. Marinopoulos and M. Grüning, in preparation.
- ¹² M. Grüning, A. Marini and X. Gonze, Nano Lett. **9**, 2820 (2009).
- ¹³ Y. Ma, M. Rohlfing and C. Molteni, Phys. Rev. B **80**, 241405 (2009).
- ¹⁴ H. A. van der Vorst Math. Comp. **39** (1982), 559
- ¹⁵ Note that in the Lanczos approach the energy range includes always the lowest energies. In principle it is possible to choose a different energy range, not necessarily containing the lowest energy, using the modification proposed by G. Grosso, L. Martinelli and G. Pastori Parravini, Phys. Rev. B **51**, 1303313038 (1995)
- ¹⁶ R. Haydock, in *Solid State Phys.*, **35** 215 (1980) edited by H. Ehrenfest, F. Seitz, and D. Turnbull, Academic Press.
- ¹⁷ M. Cini, *Topics and Methods in Condensed Matter Theory From Basic Quantum Mechanics to the Frontiers of Research* (Springer, Berlin, 2007) p. 313-316.
- ¹⁸ In particular, at each iteration both the computational cost and the storage are increasing, since all the vectors in the basis are needed to determine the new one.
- ¹⁹ In principle also the Hermitian algorithm can break down. In fact after many iterations, because of the numerical error, the vectors in the Lanczos basis may stop to be orthonormal.
- ²⁰ B. Walker, A. M. Saitta, R. Gebauer, and S. Baroni, Phys. Rev. Lett. **96**, 113001 (2006).
- ²¹ D. Rocca, R. Gebauer, Y. Saad, and S. Baroni, J. Chem. Phys. **128**, 154105 (2008).
- ²² D. Rocca, D. Lu, and G. Galli, J. Chem. Phys. **133**, 164109 (2010).
- ²³ A. Mostafazadeh, J. Math. Phys. **43**, 205 (2002).
- ²⁴ A. Mostafazadeh, J. Math. Phys. **43**, 3944 (2002).
- ²⁵ R. Zimmermann, Phys. Stat. Sol. **41**, 23 (1970).
- ²⁶ L. X. Benedict and E. L. Shirley, Phys. Rev. B **59**, 5441 (1999).
- ²⁷ For real matrices, as in the case of TD-DFT for finite systems and local exchange-correlation functionals, the cost is reduced further, since one can construct before-hand the two matrix $A = R + C$ and $B = R - C$, so that only a single matrix-vector multiplication is needed (giving another factor two). Moreover usually B reduces to a diagonal matrix, containing on the diagonal the energy differences of the particle-hole pairs. In this case the algorithm is equivalent to the one proposed by Casida, see Ref. 9.
- ²⁸ X. Gonze, J. M. Beuken, R. Caracas, F. Detraux, M. Fuchs, G. M. Rignanese, L. Sindic, M. Verstraete, G. Zerah, F. Jollet, *et al.*, Comp. Mater. Sci. **25**, 478 (2002); X. Gonze, G. M. Rignanese, M. Verstraete, J. M. Beuken, Y. Pouillon, R. Caracas, F. Jollet, M. Torrent, G. Zerah, M. Mikami, *et al.*, Z. Kristallogr. **220**, 558 (2005) X. Gonze, B. Amadon, P. M. Anglade, J. M. Beuken, F. Bottin, P. Boulanger, F. Bruneval, D. Caliste, R. Caracas, M. Côté, *et al.*, Comp. Phys. Commun. **180**, 2582 (2009).
- ²⁹ A. Marini, C. Hogan, M. Grüning and D. Varsano, Comp. Phys. Comm. **180**, 1392 (2009).
- ³⁰ Absorption measurements at a resolution of 50 cm^{-1} using a gas saturation method (298 K) by H. Scharping, C. Zetzsch, and H. A. Dessouki, J. Mol. Spectrosc. **123**, 382 (1987).
- ³¹ R. Chen, and H. Guo, Chem. Phys. Lett **369**, 650 (1997); *ibid.* J. Chem. Phys. **119**, 5762 (2003).
- ³² This corresponds to a two-bands system, with bands between $|b_u - b_g|$ and $(b_u + b_g)$, and between $-(b_u + b_g)$ and $-|b_u - b_g|$.
- ³³ The sum of the asymptotic values tends to twice the particle-hole pair energy cutoff, the difference to the optical gap of the system. See also Ref. 21.
- ³⁴ We have tested that the convergence behavior does not depend on the particular expression for the error and that the behavior resemble that of the error with respect to the exact diagonalization, at least when no terminator is used.
- ³⁵ The reason of just 1 eV difference, while the unoccupied orbital space of R' contains 25 more states, is that KS states in this energy region are in fact very close to each others.